MNRAS **000**, 1–?? (2017) Preprint 6 June 2018 Compiled using MNRAS LATEX style file v3.0

Carbon X-ray absorption in the local ISM: fingerprints in X-ray Novae spectra

Efraín Gatuzz[1⋆], J.-U. Ness[2], T. W. Gorczyca[3], M. F. Hasoglu[4], Timothy R. Kallman[5], and Javier A. García[6]
[1] *ESO, Karl-Schwarzschild-Strasse 2, D-85748 Garching bei München, Germany*
[2] *XMM-Newton Observatory SOC, European Space Astronomy Centre, Camino Bajo del Castillo s/n, Urb. Villafranca del Castillo, E-28692 Villanueva de la Cañada, Madrid, Spain*
[3] *Western Michigan University, Kalamazoo, MI 49008, USA*
[4] *Department of Computer Engineering, Hasan Kalyoncu University, 27100 Sahinbey, Gaziantep, Turkey*
[5] *NASA Goddard Space Flight Center, Greenbelt, MD 20771, USA*
[6] *Cahill Center for Astronomy and Astrophysics, California Institute of Technology, Pasadena, CA 91125, USA*

Accepted XXX. Received YYY; in original form ZZZ

ABSTRACT
We present a study of the C K-edge using high-resolution LETGS *Chandra* spectra of four novae during their super-soft-source (SSS) phase. We identified absorption lines due to C II Kα, C III Kα and C III Kβ resonances. We used these astronomical observations to perform a benchmarking of the atomic data, which involves wavelength shifts of the resonances and photoionization cross-sections. We used improved atomic data to estimate the C II and C III column densities. The absence of physical shifts for the absorption lines, the consistence of the column densities between multiple observations and the high temperature required for the SSS nova atmosphere modeling support our conclusion about an ISM origin of the respective absorption lines. Assuming a collisional ionization equilibrium plasma the maximum temperature derived from the ratio of C II/C III column densities of the absorbers correspond to $T_{max} < 3.05 \times 10^4$ K.

Key words: ISM: structure – ISM: atoms – X-rays: ISM

1 INTRODUCTION

High-resolution X-ray spectroscopy constitutes a powerful technique to study the elements associated with the local interstellar medium (ISM), defined as gas and dust between the stars. By using an X-ray bright source, acting as a lamp, the absorption features identified in the X-ray spectra provide information about the physical properties of the gas between the source and the observer. Using X-ray spectra of low mass X-ray binaries (LMXBs) the O, Fe, Ne, Mg and Si K absorption edges associated to the ISM have been analyzed in previous works (Juett et al. 2004; Ueda et al. 2005; Juett et al. 2006; Yao et al. 2009; Pinto et al. 2010, 2013; Costantini et al. 2012; Gatuzz et al. 2013a,b; Liao et al. 2013; Luo & Fang 2014; Gatuzz et al. 2014, 2015; Schulz et al. 2016; Gatuzz et al. 2016; Nicastro et al. 2016a,b; Joachimi et al. 2016; Gatuzz & Churazov 2018).

The ISM is composed of multiple phases which depends on their characteristic temperatures and densities. Carbon, which constitutes the fourth most abundant element in the Galaxy, can be used to probe the link between the different phases. C I, for example, has been used to analyze the cold Galactic gas which is characterized by a relatively low thermal pressure using the Space Telescope Imaging Spectrograph (STIS) on board the *Hubble Space Telescope* (Jenkins & Tripp 2001; Burgh et al. 2010; Jenkins & Tripp 2011), while the C II 158 μm line allows the characterization of the cold atomic clouds in transition from atomic to molecular form (Pineda et al. 2013; Langer et al. 2014; Pineda et al. 2014, 2017; Richter et al. 2017; Savage et al. 2017). Also, it has been shown that solids that contain carbon atoms, such as graphite and polycyclic aromatic hydrocarbons, may constitute the main heat source for the ISM (Draine & Li 2001; Helou et al. 2001; Okada et al. 2013; Chen et al. 2017; Shannon et al. 2018). In this sense, it is essential to estimate the amount of C depleted in the dust phase in order to fully understand the heating-cooling ISM processes.

One of the advantages of the high-resolution X-ray spectroscopy is that it provides access to both gas and solid components of the ISM. The C K-edge, located at 38-44 Å wavelength, can be accessed only through the low-energy transmission grating (LETG) on board of the *Chandra* ob-

⋆ E-mail: egatuzzs@eso.org

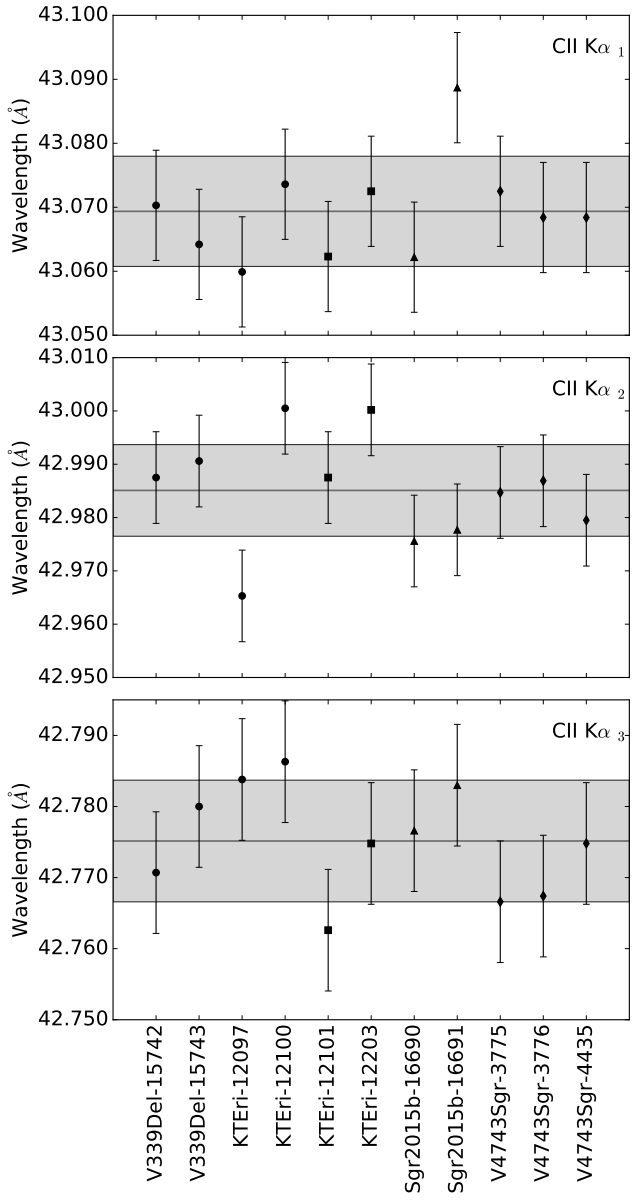

Figure 1. C II Kα resonances observational wavelengths determined from Gaussian fits. The horizontal grey region correspond to the average value and its 90% uncertainty.

servatory. Super-soft-sources (SSS) provide high count continuum spectra that can be used to perform such analysis. Although their X-ray spectra can be complex, showing spectral features due to multiple temperature components, carbon absorption features have been identified (Ness et al. 2009; Rauch et al. 2010; van Rossum 2012; Rauch 2016).

In this paper we present an analysis of the C absorption features in the ISM using *Chandra* high-resolution spectra of four sources. The outline of this paper is as follows: In Section 2 we describe the observations and data reduction. In Section 3 we describe the C K-edge modeling and the atomic data involved. In Section 4 we discuss the main results. Finally, in Section 5 we summarize our main conclusions.

2 OBSERVATIONS AND DATA REDUCTION

We analyze *Chandra* spectra of four SSS in order to study the ISM carbon K-edge along different lines of sight. Because of their brightness and proximity, SSS high-resolution spectra constitute a useful way to analyze not only the binary system involved but also the ISM fingerprints identified as absorption features. Table 1 lists the specifications for each LETGS-HRC observation, the observation date, the exposure time, the hydrogen column density 21 cm measurement from the Kalberla et al. (2005) survey, the count rate and the number of counts in the C K-α wavelength region (38–44 Å). The data were reduced using the Chandra Interactive Analysis of Observations software (CIAO,version 4.9) and following the standard procedure to obtain the Low-Energy Transmission Grating (LETG) spectra[1]. For each observation we combine the +1/-1 orders using the `combine_grating_spectra` script. We use the XSPEC analysis data package (Arnaud 1996, version 12.9.1[2]) to perform the spectral fitting. Finally, we use χ^2 statistic with the weighting method for low counts regime defined by Churazov et al. (1996)

3 C K-EDGE MODELING

In order to analyze the C K-edge absorption region (38–44 Å) we first used a functional model consisting of a power law continuum with absorption lines described by Gaussian profiles. Table 2 shows the wavelength position for all absorption lines identified in the spectra as well as their average values. Theoretical values, obtained from Hasoglu et al. (2010) calculations, are also listed. Both cameras, the High Resolution Camera (HRC) and the Advanced CCD Imaging Spectrometer (ACIS) have C I instrumental absorption at $\sim$ 43.6 Å due to absorption edges in the materials comprising the instruments, as is indicated by the Chandra Proposers' Observatory Guide[3]. We have not identified C I absorption lines in excess of instrumental features that could be associated with the ISM in the X-ray spectra sample. In this sense, it has been shown that the C I column density associated to the ISM tends to be lower than 10^{14} cm^{-2} along multiple line-of-sights, including regions with large HI column densities (Jenkins & Tripp 2011; Gerin et al. 2015; Welty et al. 2016; Pineda et al. 2017).

Figure 1 shows the wavelength positions for each resonance in the C II Kα triplet, which have been measured in all observations. It is important to note that, considering the uncertainties, the wavelength positions tend to agree not only between different observations of the same source but also for different sources. C III Kα and C III Kβ absorption lines were identified in 7 and 5 observations, respectively. Figure 2 shows the best-fit wavelength positions measured for both resonances. In both figures the horizontal gray regions indicate the average values and their uncertainties. It is clear from the plots that, considering the uncertainties, the wavelength positions do not show significant shift between observations.

[1] http://cxc.harvard.edu/ciao/threads/gspec.html
[2] https://heasarc.gsfc.nasa.gov/xanadu/xspec/
[3] http://cxc.harvard.edu/proposer/POG/html/index.html

Table 1. List of *Chandra* LETGS-HRC observations.

Source	ObsID.	Obs. date	Exp. time (ks)	N(HI) (10^{21} cm^{-2})	count-rate (counts/s)	Counts (38–44 Å)
KTEri	12097	23-01-2010	14.9	0.52	11.52	25028
	12100	31-01-2010	27.9		77.73	18737
	12101	06-02-2010	47.8		37.48	16971
	12203	21-04-2010	32.4		106.5	26717
Sgr2015b	16690	16-10-2015	48	1.11	12.07	106572
	16691	12-11-2015	50		6.41	56768
V339Del	15742	09-11-2013	46	1.23	68.31	352919
	15743	06-12-2013	49		48.34	293788
V4743Sgr	3775	19-03-2003	20.3	1.05	38.91	45173
	3776	18-07-2003	11.7		37.16	26349
	4435	25-09-2003	12.0		19.78	16209

N(HI) column densities obtained from Kalberla et al. (2005).

Table 2. Absorption line assignments with observed wavelength.

Source	ObsID.	CII			CIII	
		$K\alpha_1$ (Å)	$K\alpha_2$ (Å)	$K\alpha_3$ (Å)	$K\alpha$ (Å)	$K\beta$ (Å)
Theoretical		43.0592	42.9867	42.6818	42.2360	38.4459
KTEri	12097	43.0599 ± 0.0043	42.9653 ± 0.0043	42.7838 ± 0.0043	42.2091 ± 0.0042	38.4100 ± 0.0038
	12100	43.0736 ± 0.0039	43.0005 ± 0.0039	42.7863 ± 0.0039	–	–
	12101	43.0623 ± 0.0047	42.9875 ± 0.0047	42.7626 ± 0.0047	42.2042 ± 0.0046	–
	12203	43.0725 ± 0.0047	43.0002 ± 0.0047	42.7748 ± 0.0047	–	–
Sgr2015b	16690	43.0622 ± 0.0034	42.9756 ± 0.0034	42.7766 ± 0.0034	–	–
	16691	43.0887 ± 0.0388	42.9777 ± 0.0387	42.7830 ± 0.0385	–	–
V339Del	15742	43.0703 ± 0.0043	42.9875 ± 0.0043	42.7707 ± 0.0043	42.1873 ± 0.0042	38.4093 ± 0.0038
	15743	43.0642 ± 0.0047	42.9906 ± 0.0047	42.7800 ± 0.0047	42.1752 ± 0.0046	38.4082 ± 0.0042
V4743Sgr	3775	43.0725 ± 0.0039	42.9847 ± 0.0039	42.7666 ± 0.0038	42.1878 ± 0.0038	38.4039 ± 0.0035
	3776	43.0684 ± 0.0043	42.9869 ± 0.0043	42.7674 ± 0.0043	42.1632 ± 0.0042	–
	4435	43.0684 ± 0.0043	42.9795 ± 0.0043	42.7748 ± 0.0043	42.1615 ± 0.0042	38.4133 ± 0.0038
Average		43.0694 ± 0.0074	42.9851 ± 0.0074	42.7751 ± 0.0074	42.1840 ± 0.0043	38.4089 ± 0.0038

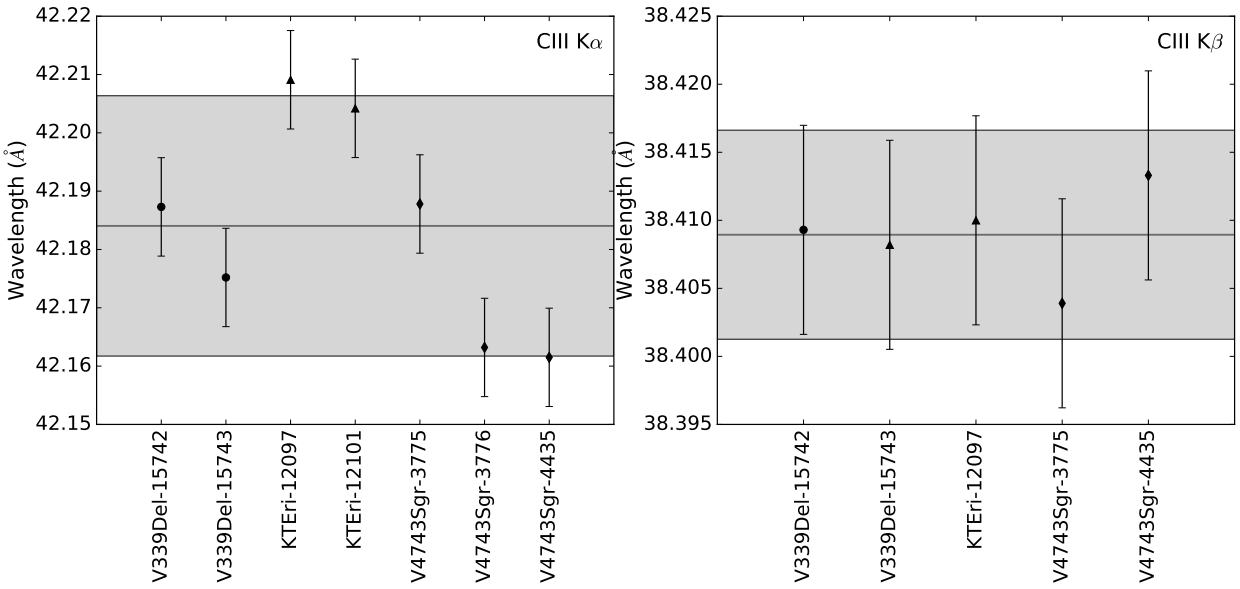

Figure 2. Left pannel: C III Kα resonance observational wavelengths determined from Gaussian fits. Right pannel: C III Kβ resonance observational wavelengths determined from Gaussian fits. The horizontal gray region corresponds to the average value and its 90% uncertainty.

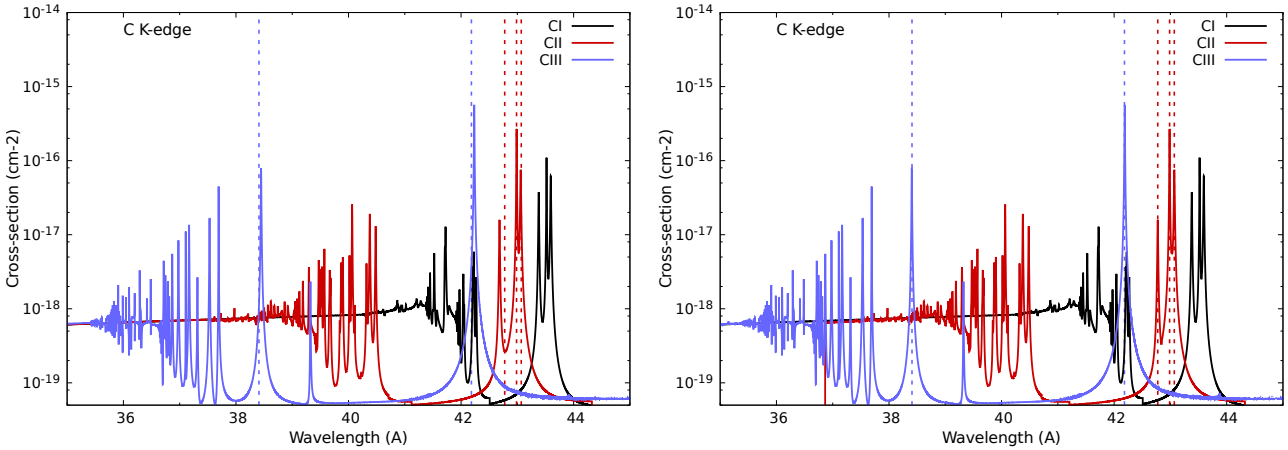

Figure 3. C I, C II and C III photoabsorption cross sections computed by Hasoglu et al. (2010) that are implemented in the `ISMabs` model. Vertical dashed lines correspond to the average measurements listed in Table 1. Left panel displays the original cross sections while right panel shows the same curves after the benchmarking.

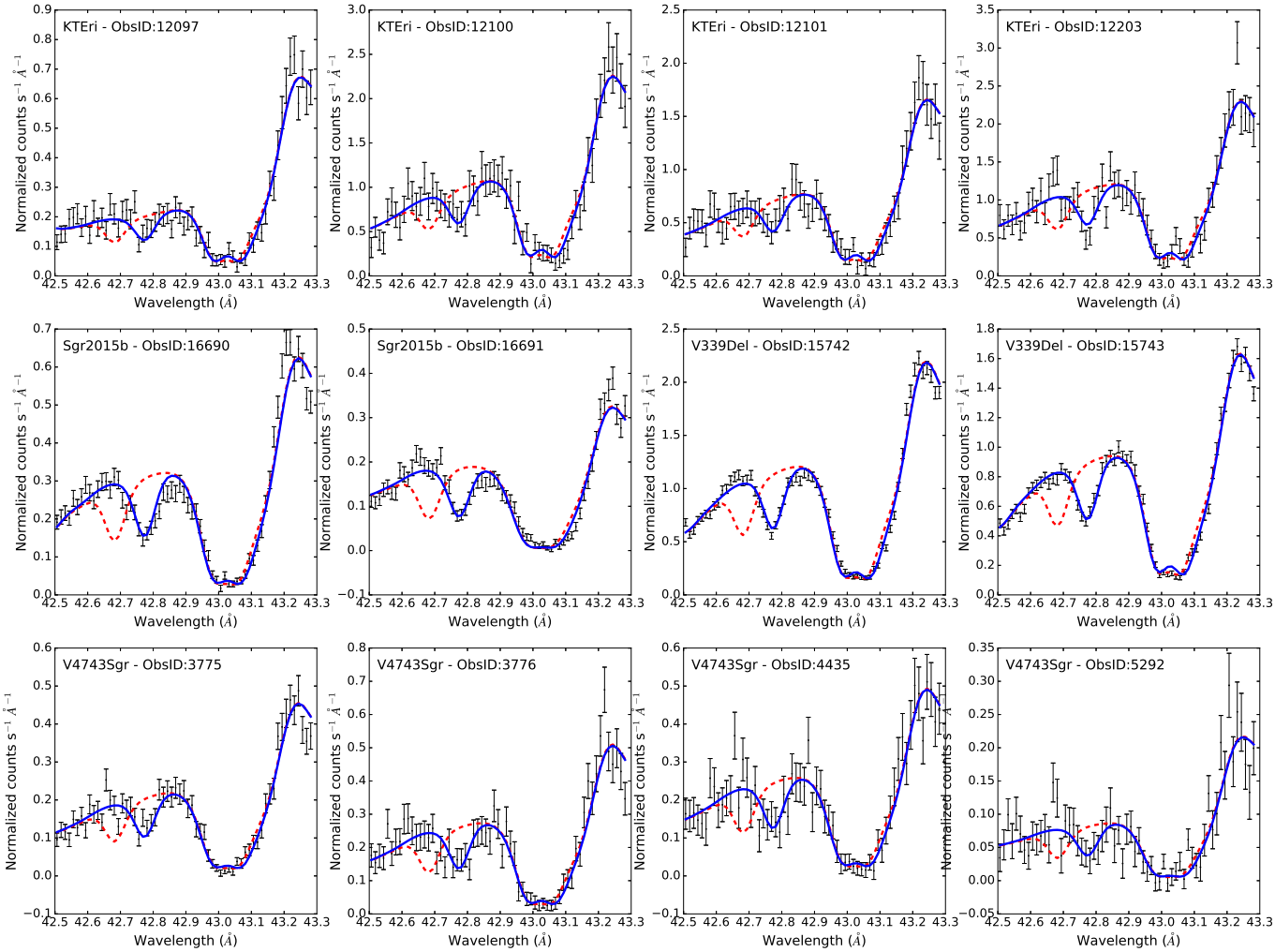

Figure 4. Best fit results using *Chandra* LETG data for the C II K-edge wavelength region. Lines correspond to the model before and after the atomic data benchmarking (red dashed and blue solid lines, respectively)

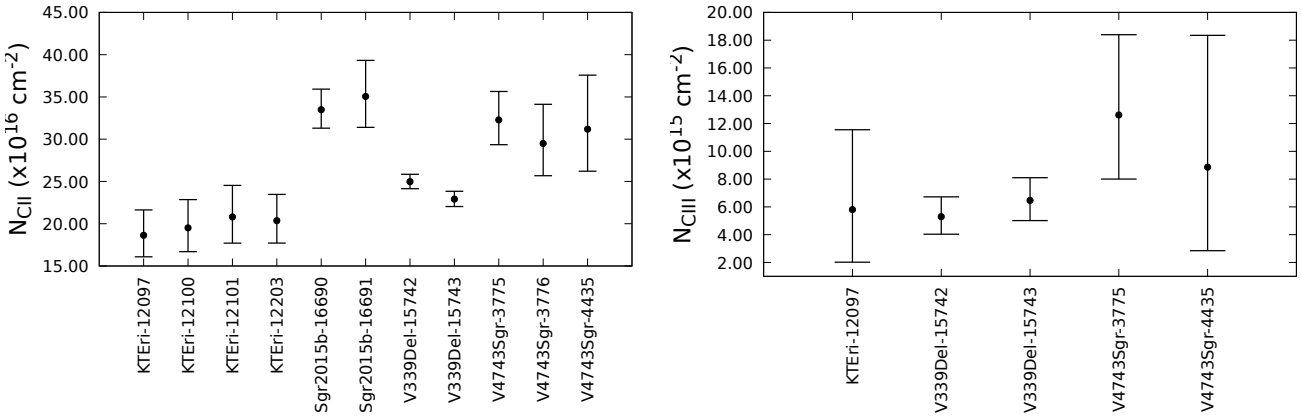

Figure 5. Left pannel: C II column densities obtained from the best `ISMabs` fit. Right pannel: C III column densities obtained from the best `ISMabs` fit.

Table 3. Column density best-fit results.

Source	ObsID.	N(CII)	N(CIII)	CII/CIII
KTEri	12097	$18.63^{+2.99}_{-2.55}$	$0.58^{+0.58}_{-0.38}$	32.12 ± 27.00
	12100	$19.51^{+3.34}_{-2.81}$		
	12101	$20.81^{+3.73}_{-3.10}$		
	12203	$20.36^{+3.11}_{-2.65}$		
Sgr2015b	16690	$33.50^{+2.43}_{-2.19}$		
	16691	$35.06^{+4.27}_{-3.66}$		
V339Del	15742	$24.98^{+0.87}_{-0.83}$	$0.53^{+0.14}_{-0.13}$	47.13 ± 12.11
	15743	$22.91^{+0.92}_{-0.88}$	$0.65^{+0.16}_{-0.15}$	35.24 ± 8.51
V4743Sgr	3775	$32.28^{+3.36}_{-2.93}$		
	3776	$29.50^{+4.64}_{-3.81}$	$1.26^{+0.58}_{-0.46}$	23.41 ± 10.24
	4435	$31.19^{+6.40}_{-4.98}$	$0.89^{+0.95}_{-0.60}$	35.04 ± 31.37

Column densities in units of 10^{16} cm^{-2}.

We performed a benchmarking of the atomic data by comparing the observed and theoretical absorption lines in the C K-edge region. Left panel in Figure 3 shows the C I (black line), C II (red line) and C III (blue line) photoabsorption cross sections computed by Hasoglu et al. (2010). Vertical lines correspond to the average measurements listed in Table 1. It is clear that the resonance positions for the Kα transitions differ between the theoretical predictions and the observational measurements. In this sense we have adjusted cross sections in order to obtain the best possible agreement with the observed lines. The shifts are +10.2 mÅ, −1.59 mÅ, and +93.3 mÅ for the C II Kα_1, Kα_2 and Kα_3 resonances, respectively. The larger shift for the Kα_3 is expected because the $n = 3$ resonances carry the greatest energy uncertainty along a Rydberg series (Hasoglu et al. 2010). For C III we move the Kα and the whole cross-section by −52 mÅ, and −37 mÅ, respectively. From the theoretical point of view, a $\sim$ 59 mÅ under-prediction in wavelength is expected (Hasoglu et al. 2010). Right panel in Figure 3 shows the cross sections after the wavelength corrections. It is important to mention that such benchmarking has been performed previously for the oxygen and neon photoabsorption cross-sections by Gatuzz et al. (2013a,b, 2015) concluding that the *Chandra* wavelength calibration can be safely used to correct the theoretical wavelength resonance positions.

4 RESULTS AND DISCUSSIONS

We included the corrected cross-sections from Hasoglu et al. (2010) in the `ISMabs`[4] model in order to estimate C II and C III column densities in the SSS spectra listed in Table 1. Figure 4 shows the best-fit results using the `ISMabs` model for the C II K-α wavelength region (42.5–43.3 Å). In each panel, black data points correspond to the observation. The model before the atomic data corrections and after the correction are indicated (red dashed and blue solid lines, respectively). In all cases we obtained a data fitting improvement of $\Delta\chi^2 > 20$. Table 3 lists the column densities obtained for each observation. Due to the elemental abundance enrichments in the ejected material from the respective novae explosion through the mixing process (Kelly et al. 2013), differences between column densities for observations performed at different epochs are expected if the absorbing material is intrinsic to the source. Figure 5 shows a comparison between the column densities obtained from the `ISMabs` model. It is clear from the plot that the column densities tend to agree for different observations of the same source. Differences between sources, on the other hand, are expected due to the density distribution of the ISM gas along the Galaxy (Robin et al. 2003; Kallman et al. 2009; Nicastro et al. 2016a,b; Gatuzz & Churazov 2018).

Another possibility is an origin in the SSS atmosphere which usually shows multiple absorption features (Orio 2012; Ness 2012; Ness et al. 2013). However, such atmospheres require high temperatures (> 0.6MK), for which we will not find C I, C II and C III ions (Ness et al. 2009; Rauch et al. 2010; van Rossum 2012; Rauch 2016). It is important to compare the 1$\sim$2 months observation separation time in our sample with the novae evolution time-scale, which can vary from months to years (Schwarz et al. 2011). For example, Ness et al. (2007) modeled the X-ray high-resolution spectra of the RS Ophiuchi novae, a source that shows a notable evolution in both, the continuum and the emission/absorption features, within months (see Figure 1 in Ness et al. 2009). The model used by Ness et al. (2007) included a compo-

[4] `https://heasarc.gsfc.nasa.gov/xanadu/xspec/models/ismabs.html`

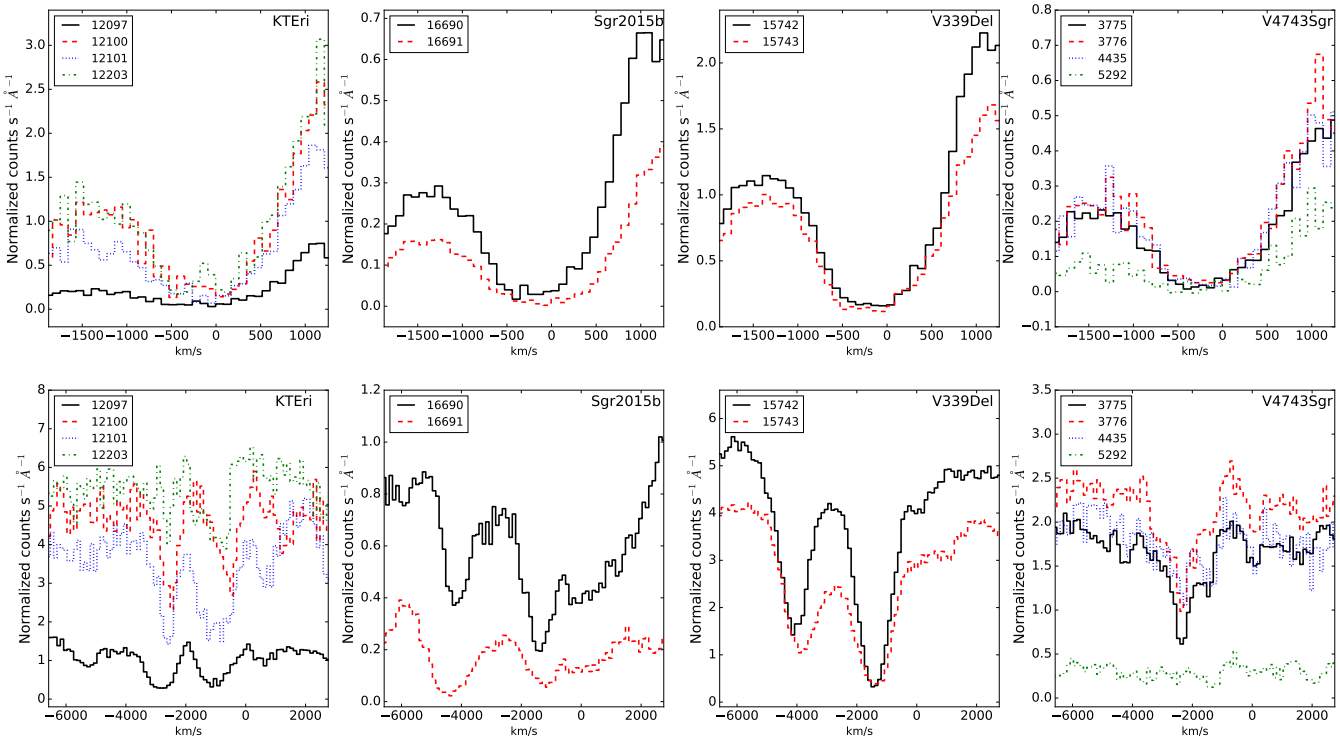

Figure 6. C II Kα_1 (top pannels) and C VI Kα (bottom pannels) absorption lines parametrized in velocity space for each source analyzed.

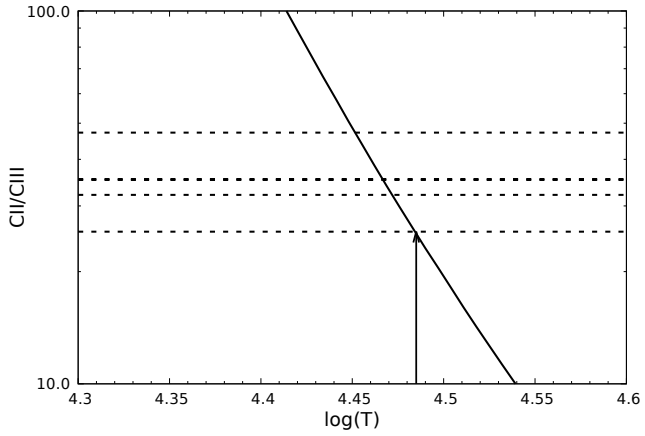

Figure 7. C II/C III ratio obtained from XSTAR calculations assuming collisional ionization equilibrium plasma. Horizontal dashed lines correspond to the ratios listed in Table 3. The arrow indicates the maximum temperature obtained.

nent for the ISM local absorption and a second component to model the circumstellar material intrinsic to the source. The best-fit requires that the oxygen contribution from the circumstellar material disappears around day 54 after the outburst, probably due to photoionization of the local gas by the radiation field.

Figure 6 shows a comparison between C II Kα_1 (top pannels) and C VI Kα (bottom pannels) absorption lines parametrized in velocity space for each source analyzed in this work. The C VI Kα absorption line has been identified as intrinsic to the source previously (Ness et al. 2003; Petz et al. 2005; Ness et al. 2007; Ness 2012; van Rossum 2012). It is clear from the plot that the C II Kα_1 remains at the same wavelength while there are no C VI Kα absorption features at rest wavelength. Also, some high-resolution X-ray novae spectra have shown P Cygni profiles (Ness et al. 2007; Orio et al. 2013) which we have not identified in the analyzed spectra.

It is important to note that there is no a reliable method to determine the total amount of carbon emitted in X-ray ejecta, in order to compare with the ISM abundance. Theoretical estimation, such as Rauch et al. (2010), depends on multiple factors including the composition of the accreted material, nuclear burning products, composition of the white dwarf and the amount of mixing of white dwarf material into the ejecta.

Table 3 also list the C II/C III ratios for those sources for which both column densities can be estimated. It is clear that C II dominates in all cases. In this sense, previous analysis using *Herschel* Galactic observations show that C II constitutes the main carbon reservoir along the lines of sight in most cases (Pineda et al. 2014; Gerin et al. 2015). The ion fractions depend on the physical state of the plasma. We used the XSTAR[5] code to estimate the maximum temperature of the gas assuming collisional ionization equilibrium (see Gatuzz & Churazov 2018). Figure 7 shows the C II/C III ra-

[5] https://heasarc.gsfc.nasa.gov/lheasoft/xstar/xstar.html

tio obtained from the XSTAR calculations. Horizontal dashed lines correspond to the ratios listed in Table 3 while the vertical arrow indicates the maximum temperature derived. We found $T_{max} < 3.05 \times 10^4$ K.

5 CONCLUSIONS AND SUMMARY

We have performed an analysis of the C K-edge using high-resolution *Chandra* spectra of four SSS. The instrumental features due to a C layer in the camera prevent the analysis of C I absorption. We have detected all three resonances of the C II Kα in 11 observations as well as the C III Kα and Kβ in 7 and 5 observations, respectively. We used the astronomical observations in order to perform a benchmarking of the atomic data computed by Hasoglu et al. (2010). We have included these corrected cross-sections in the `ISMabs` X-ray absorption model. Using the improved atomic data we estimated the C II and C III column densities for each observation. While high-ionized lines such as C VI Kα show significant shifts between different observations and different sources, the C II and C III wavelength positions are consistent. The absence of physical shifts for the absorption lines, the lack of variability for the column densities between different observations and the low temperatures associated to these ions compared to X-ray novae typical atmosphere temperature support our conclusion about an ISM origin of the absorption lines identified in the spectra. From the ratios of C II/C III column densities, we found $T_{max} < 3.05 \times 10^4$ K, which corresponds to the so-called warm component of the ISM.

ACKNOWLEDGEMENTS

We are grateful to the referee, Dr. Lia Corrales, for the careful reading of our manuscript and the valuable comments that led to improvements of its scientific content.

REFERENCES

Arnaud K. A., 1996, in Jacoby G. H., Barnes J., eds, Astronomical Society of the Pacific Conference Series Vol. 101, Astronomical Data Analysis Software and Systems V. p. 17
Burgh E. B., France K., Jenkins E. B., 2010, ApJ, 708, 334
Chen X. H., Li A., Zhang K., 2017, ApJ, 850, 104
Churazov E., Gilfanov M., Forman W., Jones C., 1996, ApJ, 471, 673
Costantini E., et al., 2012, A&A, 539, A32
Draine B. T., Li A., 2001, ApJ, 551, 807
Gatuzz E., et al., 2013a, ApJ, 768, 60
Gatuzz E., et al., 2013b, ApJ, 778, 83
Gatuzz E., García J., Mendoza C., Kallman T. R., Bautista M. A., Gorczyca T. W., 2014, ApJ, 790, 131
Gatuzz E., García J., Kallman T. R., Mendoza C., Gorczyca T. W., 2015, ApJ, 800, 29
Gatuzz E., García J. A., Kallman T. R., Mendoza C., 2016, A&A, 588, A111
Gatuzz E., Churazov E., 2018, MNRAS, 474, 696
Gerin M., et al., 2015, A&A, 573, A30
Helou G., Malhotra S., Hollenbach D. J., Dale D. A., Contursi A., 2001, ApJ, 548, L73
Hasoglu M. F., Abdel-Naby S. A., Gorczyca T. W., Drake J. J., McLaughlin B. M., 2010, ApJ, 724, 1296
Jenkins E. B., Tripp T. M., 2001, ApJS, 137, 297
Jenkins E. B., Tripp T. M., 2011, ApJ, 734, 65
Joachimi K., Gatuzz E., García J. A., Kallman T. R., 2016, MNRAS, 461, 352
Juett A. M., Schulz N. S., Chakrabarty D., 2004, ApJ, 612, 308
Juett A. M., Schulz N. S., Chakrabarty D., Gorczyca T. W., 2006, ApJ, 648, 1066
Kalberla P. M. W., Burton W. B., Hartmann D., Arnal E. M., Bajaja E., Morras R., Pöppel W. G. L., 2005, A&A, 440, 775
Kallman T. R., Bautista M. A., Goriely S., Mendoza C., Miller J. M., Palmeri P., Quinet P., Raymond J., 2009, ApJ, 701, 865
Kelly K. J., Iliadis C., Downen L., José J., Champagne A., 2013, ApJ, 777, 130
Langer W. D., Velusamy T., Pineda J. L., Willacy K., Goldsmith P. F., 2014, A&A, 561, A122
Liao J.-Y., Zhang S.-N., Yao Y., 2013, ApJ, 774, 116
Luo Y., Fang T., 2014, ApJ, 780, 170
Ness J.-U., et al., 2003, ApJ, 594, L127
Ness J.-U., et al., 2007, ApJ, 665, 1334
Ness J.-U., et al., 2009, AJ, 137, 3414
Ness J. U., 2012, Bulletin of the Astronomical Society of India, 40, 353
Ness J.-U., et al., 2013, A&A, 559, A50
Nicastro F., Senatore F., Gupta A., Guainazzi M., Mathur S., Krongold Y., Elvis M., Piro L., 2016a, MNRAS, 457, 676
Nicastro F., Senatore F., Gupta A., Mathur S., Krongold Y., Elvis M., Piro L., 2016b, MNRAS, 458, L123
Okada Y., et al., 2013, A&A, 553, A2
Orio M., 2012, Bulletin of the Astronomical Society of India, 40, 333
Orio M., et al., 2013, MNRAS, 429, 1342
Petz A., Hauschildt P. H., Ness J.-U., Starrfield S., 2005, A&A, 431, 321
Pineda J. L., Langer W. D., Velusamy T., Goldsmith P. F., 2013, A&A, 554, A103
Pineda J. L., Langer W. D., Goldsmith P. F., 2014, A&A, 570, A121
Pineda J. L., et al., 2017, ApJ, 839, 107
Pinto C., Kaastra J. S., Costantini E., Verbunt F., 2010, A&A, 521, A79
Pinto C., Kaastra J. S., Costantini E., de Vries C., 2013, A&A, 551, A25
Rauch T., 2016, in Deustua S., Allam S., Tucker D., Smith J. A., eds, Astronomical Society of the Pacific Conference Series Vol. 503, The Science of Calibration. p. 193
Rauch T., Orio M., Gonzales-Riestra R., Nelson T., Still M., Werner K., Wilms J., 2010, ApJ, 717, 363
Richter P., et al., 2017, A&A, 607, A48
Robin A. C., Reylé C., Derrière S., Picaud S., 2003, A&A, 409, 523
Savage B. D., et al., 2017, ApJS, 232, 25
Schulz N. S., Corrales L., Canizares C. R., 2016, ApJ, 827, 49
Schwarz G. J., et al., 2011, ApJS, 197, 31
Shannon M. J., Peeters E., Cami J., Blommaert J. A. D. L., 2018, ApJ, 855, 32
Ueda Y., Mitsuda K., Murakami H., Matsushita K., 2005, ApJ, 620, 274
Welty D. E., Lauroesch J. T., Wong T., York D. G., 2016, ApJ, 821, 118
Yao Y., Schulz N. S., Gu M. F., Nowak M. A., Canizares C. R., 2009, ApJ, 696, 1418
van Rossum D. R., 2012, ApJ, 756, 43